

Supplementary Material

Supplementary Methods

Isolation of primary pulmonary vascular cells

Primary pulmonary endothelial cells (ECs) and/or smooth muscle cells (SMCs) were isolated from pulmonary arteries (PA) as previously described (1, 2) and as briefly summarized below.

Isolation of human pulmonary artery ECs and SMCs

Human PA tissue samples were collected in RPMI-1640 sample buffer (Gibco, 11530586) containing 1% penicillin and streptomycin (P/S, Thermo Fischer, 11548876). For PA EC isolation, PA samples were placed into Petri dishes (Corning, 3295) coated with 0.1% gelatin (Pan Biotech, P0-20410). Using a scalpel, cells were scraped from the intima onto the dish surface. Petri dishes were immediately filled with 5 mL complete EC medium (cECM, Sciencell, 1001) and incubated at 37°C. EC medium was exchanged every 2 days. For isolation of PA SMCs, the medial layer of PA tissue samples was cut into 2x2 mm pieces and placed into coated Petri dishes into which a crosshatch pattern had been scratched. Tissue pieces were left to dry onto the dish surface for 15 min and then covered with DMEM/F-12 (Gibco, 11320033, hereafter referred to as DMEM) containing 10% of fetal bovine serum (FBS) and 1% P/S. PA tissue pieces were removed after 7 days, followed by medium exchange every 2 days.

Purification of ECs from mixed cultures

To eliminate fibroblasts from EC cultures, CD144⁺ ECs were purified using MACS magnetic cell separation. Cells were detached using trypsin, suspended in M199 medium (Pan Biotech, P04-07500) containing 5% FBS and 1% P/S, and centrifuged at 300g and 4°C for 7 min. Supernatant was removed, remaining cells were resuspended in 80 µl M199 medium and 20 µl CD144 microbead solution (Miltenyi Biotec, 130-097-857), and incubated at 4°C for 15 min while spinning. Next, cells were resuspended in M199 medium, pipetted into a separation column (Miltenyi Biotec, 130-042-401), and rinsed three times with M199 wash buffer (containing 1% P/S). Lastly, cECM was added into the separation column and remaining CD144⁺ cells were pressed into a culture flask, followed by incubation at 37°C.

Isolation of rat pulmonary artery SMCs

In each experimental group, PA SMCs were extracted from four randomly selected rats immediately after euthanasia. Following excision and rinsing in cold Dulbecco's phosphate-buffered saline (DPBS, 12559069), PA samples were fragmented into approximately 1x1 mm pieces, aspirated in 3 mL of DMEM (Gibco, 11320033) supplemented with 20% FBS and 1% P/S, and transferred into a T25 culture flask. The flask was then incubated at 37°C. The SMCs were checked for expansion after a 5-day incubation period, the tissue was discarded, and the culture medium was exchanged every two days thereafter.

Production of a decellularized endothelial ECM (dECM)

Primary isolated PA ECs from control, LHD w/o PH, and PH-LHD patients were seeded at confluency into 12-well or 6-well plates, respectively, and incubated at 37°C until seven days

post-confluency (with media exchange every 2 days). Cell medium was removed, and distilled water was added into each well (400 μ l into 12-well plates and 800 μ l into 6-well plates). Plates were kept at -80°C for 30 min and then thawed in 37°C for 30-45 s. This process was repeated three times. Distilled water and cell debris were aspirated and decellularized matrices were reseeded with primary cells. A >90% decellularization efficiency was confirmed by DAPI staining (Suppl. Fig. 2A-B).

dECM characterization

Surface mechanical properties as determined by atomic force microscopy

To measure the Young's modulus (E) of the endothelial dECM surface, the Petri dishes containing dECM in phosphate buffered saline (PBS) were warmed to 37°C, and the temperature was maintained throughout the experiment. Atomic force microscopy (AFM) measurements were operated in force spectroscopy contact mode. A triangular silicon nitride pyramidal tip attached to cantilevers with a nominal spring constant (k) of 0.03 N/m (MLCT-D, Bruker, Mannheim, Germany) was used to map the sample surface. Calibration of k of the cantilever was done on a bare Petri dish filled with PBS at 37°C by the thermal method using the Lorentz oscillator model prior to measurement of the samples' surfaces. A z-length of 6 μ m, a speed rate of 6 μ m/s and a trigger force (set point) of 0.3 nN were used for AFM measurements. Force (F) was calculated from the cantilever deflection (d) by means of Hook's Law ($F = \frac{1}{4} \times k \times d$) and force-displacement (F-z) curves were recorded. The surface Young's modulus E of the samples was calculated by fitting the contact part of the curves to a standard Sneddon model for a pyramidal indenter (tip) with a Poisson's ratio of 0.5. Spectroscopy force measurements were done over the entire scan area of 10 x 10 μ m with an array of 6 x 6 (36 points) or 8 x 8 (64 points) of F-z curves. Three different scan areas for each sample with three different measuring points were considered for the final calculations. For each point on the grid, one or two sets of F-z curves were collected. All data were processed using the JPK Instruments AFM software (JPK data processing software).

Mass spectrometry

Endothelial dECM were prepared as described above, and ECM proteins were harvested using lysis buffer. Protein solution was snap-frozen and thawed in 3 cycles and then heated at 95°C for 10 min. Fifty μ g protein from each sample were processed using the SP3 clean-up and digestion protocol as previously described (3). Briefly, samples were reduced for 30 min in 10 mM dithiothreitol, alkylated in 50 mM chloroacetamide for 30 min and quenched with 20 mM dithiothreitol. After dilution in acetonitrile (final concentration 70%), 500 μ g SP3 beads were added to each sample, followed by 20 min incubation on a rotor wheel. Samples were washed twice with 70% ethanol and once with 100% acetonitrile using a magnetic rack. Beads were resuspended in digestion buffer (50 mM ammonium bicarbonate, 1 μ g sequence grade trypsin (Promega), 1 μ g endopeptidase LysC (Wako, Japan)) and incubated over night at 37°C. The supernatant was collected, acidified with formic acid (final concentration 1%) and peptides were cleaned up and stored using the StageTips protocol (4).

Peptides were analyzed on an Orbitrap Exploris 480 instrument (Thermo) using data-independent acquisition (DIA). Samples were separated on a 20 cm reversed-phase column (ReproSil-Pur C18-AQ; 1.9 μ m, Dr. Maisch GmbH) using a 98 min gradient with a 250 nl/min

flow rate of increasing Buffer B concentration (from 2% to 60%) on a High-Performance Liquid Chromatography (HPLC) system (ThermoScientific). The column temperature was maintained at 45 °C using a column oven. The mass spectrometer was operated in positive polarity mode and the samples were acquired with a DIA method as described before (5). Briefly, the method consisted of an MS1 scan (m/z , 300–1,650) with an AGC target of 300% and a maximum injection time of 20 ms ($R = 120,000$). DIA scans were acquired with variable isolation window sizes at $R = 30,000$, with an AGC target of 300% and a maximum injection time of 35 ms. The spectra were recorded in profile mode, and the stepped collision energy was set to 26, 29 and 32. Data analysis was performed in Spectronaut (v. 14.3) using the library-free direct DIA approach and Q value sparse standard settings. Protein groups with at least three MS2 evidence were considered for quantification. Statistical analyses with 6 replicates per experimental group were performed in Perseus (v. 1.6.2.1) using Student's t-test.

Cell migration assay

In vitro assessment of SMC migration was performed in a wound-healing assay (6). Primary PA SMCs (isolated as described above) were cultured in 6-well plates until reaching confluency. To induce a wound, a 200 μ l pipette tip was firmly applied against the culture well, creating a scratch across the cell layer in a swift vertical motion. Subsequently, the cell media and debris were meticulously aspirated, and fresh media was gently pipetted into the corner of the well. An initial image was captured immediately after the scratch (0 h) on an EVOS M5000 microscope (Thermo Fischer, AMF5000), followed by another image taken after an 8-hour incubation period at 37°C. Migration rates were calculated from measured wound areas at 0 h and 8 h as described by Grada et al. (7).

Immunofluorescent staining and confocal scanning microscopy

Human PA tissue preserved with optimal cutting temperature (OCT) medium or rat PA tissue embedded in paraffin were sectioned into 10 μ m slices using a Microm HM 560 cryostat (Thermo Fisher) or the rotatory microtome HistoCore BIOCUT (Leica), respectively. PA cryosections or primary PA SMCs cultured on coverslips until reaching confluency were fixed with 4% paraformaldehyde (Polysciences, 50-00-0) for 10 minutes, followed by three 10-minute washes in 1x PBS (Fisher Bioreagents, BP39920). Immunofluorescent staining was performed following the protocol described in (8), using antibodies at dilutions listed in **Suppl. Tables 1 and 2**. To visualize F-actin, cells were incubated with fluorescently labelled phalloidin (Thermo Fischer, A22287) for 1 h at room temperature (RT) in a light-protected environment. After incubation, cells were washed three times for 10 min each with 1x PBS. For visualizing cell nuclei, samples were stained with 1 mg/mL DAPI (Sigma Aldrich, D9542) or DRAQ5 (Abcam, ab108410) in PBS. Tissue sections and cells were mounted using Mowiol (81381-50G, Sigma Aldrich) prepared according to the Cold Spring Harbor Protocols. Briefly, 2.4 g of Mowiol 4-88 was mixed with 6 g of glycerol (Roth, 3783.1) and 6 mL of deionized water, stirred at room temperature for several hours, heated to 50°C after adding 12 mL of 0.2 M Tris-Cl (pH 8.5), and stirred until complete dissolution of Mowiol. All histological slides were stored under light-protected conditions at 4°C for long-term preservation. Tissue and cell samples were imaged by scanning confocal microscopy (A1Rsi+, Nikon). Second harmonic generation imaging was performed on a Leica SP5 II microscope as described in (8).

Electron microscopy

Human PA samples were fixed with 2.5% glutaraldehyde in 0.1 M sodium cacodylate buffer (both Serva) for 30 min at RT and stored at 4°C. Post fixation was performed with 1% osmium tetroxide (Electron Microscopy Sciences) and 0.8% potassium ferrocyanide II (Roth) in 0.1 Mol/L cacodylate buffer for 1.5 h followed by dehydration of the samples by incubation in increasing concentrations of ethanol and embedding in Epon resin (Roth). PA ultrastructure was examined using a Zeiss EM 906 electron microscope at 80 kV acceleration voltage (Carl Zeiss).

Western blotting

EC lysates were prepared and analyzed by Western blotting as previously described (8). Antibodies were used in dilutions as listed in **Suppl. Tables 1 and 2**.

Assessment of cell proliferation

PA SMC proliferation was analyzed from single focal plane confocal microscopy images of Ki67-stained primary isolated SMCs. The rate of cell proliferation was calculated as number of Ki67+ cells relative to total cell number (determined as DAPI+ cells).

YAP1 inhibition

YAP1 inhibition in vitro

For YAP1 inhibition, SMCs were seeded into 12-well or 6-well plates and, after reaching confluency, were treated with DMEM/F-12 (Gibco, 11320033, hereafter referred to as DMEM) containing 1 mM VP (Medchem Express, CL 318952) for 3 days. For siRNA-mediated YAP1 silencing, SMCs were seeded into 12-well or 6-well plates and at 70-90% confluency were transfected with 200 mM siYAP1 (AM16708, Thermo Fischer) using Lipofectamine 200 transfection reagent (Invitrogen, 11668027) for 72 h. Transfection of a scrambled siRNA (control siRNA) served as control.

YAP1 inhibition in vivo

The effect of YAP1 inhibition on PA SMC behavior was addressed in biomaterials from rat experiments with approval by the local governmental animal care use committee (Landesamt für Gesundheit und Soziales (LaGeSO), Berlin) under protocol number G0030/18. Animal experiments were performed according to the ARRIVE guidelines and the "Guide for the Care and Use of Laboratory Animals" (Institute of Laboratory Animal Resources, 8th edition 2011). YAP1 was inhibited in either AoB or sham operated rats by repeated injections of VP (i.p. in 10 mg/kg BW) twice a week for the time interval between 3 and 9 weeks post-surgery (for study scheme please see **Suppl. Fig. 6**). Hemodynamic data for VP- or vehicle-treated AoB and sham rats has been previously published by us in an independent paper (9). Specifically, we could show that VP treatment in AoB rats (i) reduced right ventricular systolic pressure (25.9 ± 2.3 mmHg, $n=11$ in AoB-VP rats vs. 35.1 ± 4.5 mmHg, $n=10$ in AoB-vehicle rats, $p < 0.0001$), (ii) attenuated right ventricular hypertrophy assessed as right ventricular weight relative to body weight (0.0052 ± 0.000081 , $n=11$ in AoB-VP rats vs. 0.00061 ± 0.00084 , $n=11$ in AoB-vehicle

rats, $p=0.033$), and (iii) increased PA radial strain (0.47 ± 0.07 , $n=9$ in AoB-VP rats vs. 0.34 ± 0.02 , $n=8$ in AoB-vehicle rats, $p<0.0001$).

Data analyses and statistics

ImageJ 2.3.0/1.53q (10) was used for image analyses and Qlucore Omics Explorer (version 3.8) for analysis of mass spectrometric data. Figures and schemes were created using Adobe Photoshop (version 24.6.0), Adobe Illustrator (version 27.7), and BioRender. GraphPad Prism 10 (version 10.0.0) was used for statistical analyses. For two group comparisons a two-tailed unpaired Mann-Whitney U-test was used, and for comparisons between three or more groups an unpaired Kruskal-Wallis test with Dunn's correction was applied. The relationship between two variables was assessed using Spearman's correlation. A p-value of ≤ 0.05 was considered to indicate a statistically significant difference. All data are presented as mean+SD.

For plotline analyses an ImageJ macro was developed in FIJI (10) to collect pixel intensities along a line profile across multi-layer microscopy images. The macro makes use of the internal ImageJ 'Plot Profile' function to determine the pixel intensities along a user-defined line across any section of the microscopy image (10). The intensity analysis along this user-defined line is applied to all layers of a multi-layer image.

Intimal width was analyzed from single focal plane confocal microscopy images of COL4/SMA-stained human PA samples by measuring the length from the luminal vessel edge to the inner elastic laminae in $n=7-8$ biologically independent samples per group (with $n=3-6$ technical replicates per sample).

Intimal cell number was quantified on single focal plane images of COL4/SMA-stained human PA samples by counting the number of DAPI-positive nuclei in the intimal region (defined as region between the lumen and the inner elastic lamina) relative to the lumen length in $n=6$ biologically independent samples per group (with $n=3-5$ technical replicates per sample).

COL4 and LAM signals in human PA were analyzed from single focal plane images of COL4 or LAM-stained samples ($n=6$ biologically independent samples per group). COL4 and LAM signals were only measured in the intimal region (defined as region between the lumen and the inner elastic lamina). Lumen length was measured, and a ratio was calculated for COL4 or LAM signal intensity over 10 μm lumen length, respectively. The same analysis was applied for rat PAs ($n=7-9$ biologically independent samples per group).

Colocalization of the BM with either ECs or SMCs was analyzed from single focal plane images of PAs co-stained for either COL4 and CD31 or COL4 and SMA, respectively ($n=3$ biologically independent samples per group). Using the plotline macro, a 30 μm line segment was drawn from the edge of the lumen perpendicularly through the vessel wall, along which COL4, CD31, and SMA signal intensities were measured, respectively.

PA SMC migration was analyzed from brightfield microscopy images of *in vitro* wound healing assays performed with primary isolated SMCs ($n=4$ biologically independent samples per group with $n=3$ technical replicates per sample). Rate of migration was calculated by measuring the wound area immediately after application of the scratch and after 8 h using the algorithm by Grada and colleagues (7). This analysis was similarly applied to assess the effect of VP-treatment on human PA SMC migration in $n=4$ biologically independent samples per group (with $n=3$ technical replicates per sample), the effect of VP-treatment on primary isolated rat PA SMCs in $n=4$ biologically independent samples per group (with $n=3$ technical replicates

per sample), the effect of siRNA-mediated YAP1 knockdown in human PA SMCs (n=4 biologically independent samples per group, with n=3 technical replicates per sample).

The effect of *in vivo* VP-treatment on nuclear localization of YAP1 was analyzed from single focal plane images of rat PA SMCs immunostained for YAP1 by measuring the area of the YAP1 signal in DAPI-positive nuclei in n=4 biologically independent samples per group (with n=3-5 technical replicates per sample). The same analysis was applied to assess the effect of *in vitro* VP-treatment on human PA SMCs in n=10 biologically independent samples per group (with n=2 technical replicates per sample), the effect of matrix stiffness on human control PA SMCs in n=6 biologically independent samples per group (with n=2 technical replicates per group), and the effect of siRNA knockdown of YAP1 on human PA SMCs in n=6 biologically independent samples per group (with n=3 technical replicates per sample).

Gap formation was analyzed from maximum intensity projection confocal microscopy images of COL4/SMA-stained PA samples obtained from rats which had been treated with VP *in vivo* (n=7-9 animals per group). Total lumen length as well as the length of COL4-negative segments along the lumen edge (defined as gaps) were measured and the ratio of gap formation/total lumen length was calculated.

Focal adhesions and actin stress fibers were analyzed using maximum intensity projection confocal microscopy images of primary human PA SMCs stained with anti-paxillin and anti-vinculin antibodies or phalloidin, respectively. Total signal intensity was measured in n=4 biologically independent samples per group with n=3 technical replicates per sample. The intensity was normalised to the number of cells detected using DAPI to stain the cell nuclei.

Supplementary Figure Legends

Suppl. Figure 1. PA SMC migration and proliferation in left heart disease

A, Representative images in *in vitro* wound-healing assays performed on primary isolated PA SMCs of control, LHD w/o PH, or PH-LHD patients taken at 0h and 8h after the scratch. **B**, Representative confocal microscopy images of primary isolated PA SMCs of control, LHD w/o PH, and PH-LHD patients immunostained for the cell proliferation marker Ki67. Cell nuclei are visualized by DAPI (**B**). Scale bars represent 100 μm (**A**, **B**).

Suppl. Figure 2. EC decellularization efficiency

A, Representative confocal microscopy images of primary isolated PA ECs from control, LHD w/o PH, and PH-LHD patients taken prior to and after decellularization. **B**, Bar graph (mean+SD) shows efficiency of decellularization as assessed by total cell number prior to and after decellularization in control (n=4), LHD w/o PH (n=4), and PH-LHD (n=4) EC samples (all data sets based on 3 technical replicates per sample). Cell nuclei are visualized by DAPI (**A**). Scale bars represent 50 μm (**A**). Statistics: Mann-Whitney-U Test (**B**); *p*-values for statistical significance are given.

Suppl. Figure 3. Original blots presented in Figure 2

Complete unprocessed blots for representative cropped blots shown in Figure 2I'. Rectangles indicate cropped regions (control in black, LHD w/o PH in blue, and PH-LHD samples in red), ladder indicates protein molecular weight, loaded samples: primary ECs isolated from PA specimens of either healthy-heart donors (control, indicated as samples C1-C4), patients with LHD w/o PH (indicated as samples L1-L4), and patients with PH-LHD (indicated as samples P1-P4).

Suppl. Figure 5. Effect of YAP1 silencing on PA SMC migration and proliferation

A, Representative confocal microscopy images of primary isolated PA SMCs from control patients, immunostained for YAP1 following treatment with either YAP1 siRNA or control siRNA, respectively, relative to untreated controls. **B**, Bar graph (mean+SD) shows quantification of nuclear YAP1 in n=6 biologically independent samples. **C**, Representative images of *in vitro* wound healing assays performed on primary isolated control PA SMCs treated with either YAP1 siRNA or control siRNA relative to untreated controls. **D**, Bar graph (mean+SD) shows quantification of cell migration in n=6 biologically independent samples. **E**, Representative confocal microscopy images of primary isolated PA SMCs from control patients, immunostained for the proliferation marker Ki67 following treatment with either YAP1 siRNA or control siRNA relative to untreated controls. **F**, Bar graph (mean+SD) shows quantification of cell proliferation rate (assessed as percentage of Ki67-positive cells) in n=6 biologically independent samples. Cell nuclei are visualized by DAPI (**A**, **E**). Scale bars represent 100 μm (**A**, **E**) or 150 μm (**C**). Statistics: Kruskal-Wallis test with Dunn's correction for multiple comparisons (**B**, **D**, **F**); *p*-values for statistical significance are given.

Suppl. Figure 6. Effect of remodelled endothelial dECM on PA SMC migration and proliferation

A-B, Representative images of *in vitro* wound healing assays performed on primary isolated PA SMCs from LHD w/o PH patients in the absence (untreated, **A**) or presence of the YAP1 inhibitor VP (**B**). Cells were cultured on either gelatin (baseline) or dECM produced by ECs isolated from PAs of control subjects and LHD w/o PH or PH-LHD patients. **C-D**, Representative confocal microscopy images of primary isolated PA SMCs from LHD w/o PH SMCs patients in the absence (untreated, **C**) or presence of the YAP1 inhibitor VP (**D**). Cells were cultured on either gelatin (baseline) or dECM produced by ECs isolated from PAs of control subjects and LHD w/o PH or PH-LHD patients, and immunostained for the proliferation marker Ki67. Cell nuclei are visualized by DAPI. Scale bars represent 150 μm (**A**, **B**) and 200 μm (**C**, **D**), respectively.

Suppl. Figure 7. Experimental scheme for *in vivo* YAP1 inhibition in PH-LHD rats

A, Schematic shows experimental protocol for *in vivo* YAP1 inhibition. Sham-operated and AoB-operated rats were injected intraperitoneally with either DMSO (vehicle) or Verteporfin (VP, 10 mg/kg BW) twice a week for the time interval between 3 and 9 weeks post-surgery. All animals were sacrificed after week 9 for end-point analyses (PA collection for histological analysis and SMC isolation).

Suppl. Video. *In vitro* deposition of COL4 by PA ECs

Confocal microscopy video shows PAEC monolayer with deposited COL4. Cell nuclei are visualized by DAPI in blue, EC marker CD31 in red, and BM marker COL4 in green.

Suppl. Table 1

Primary and conjugated antibodies

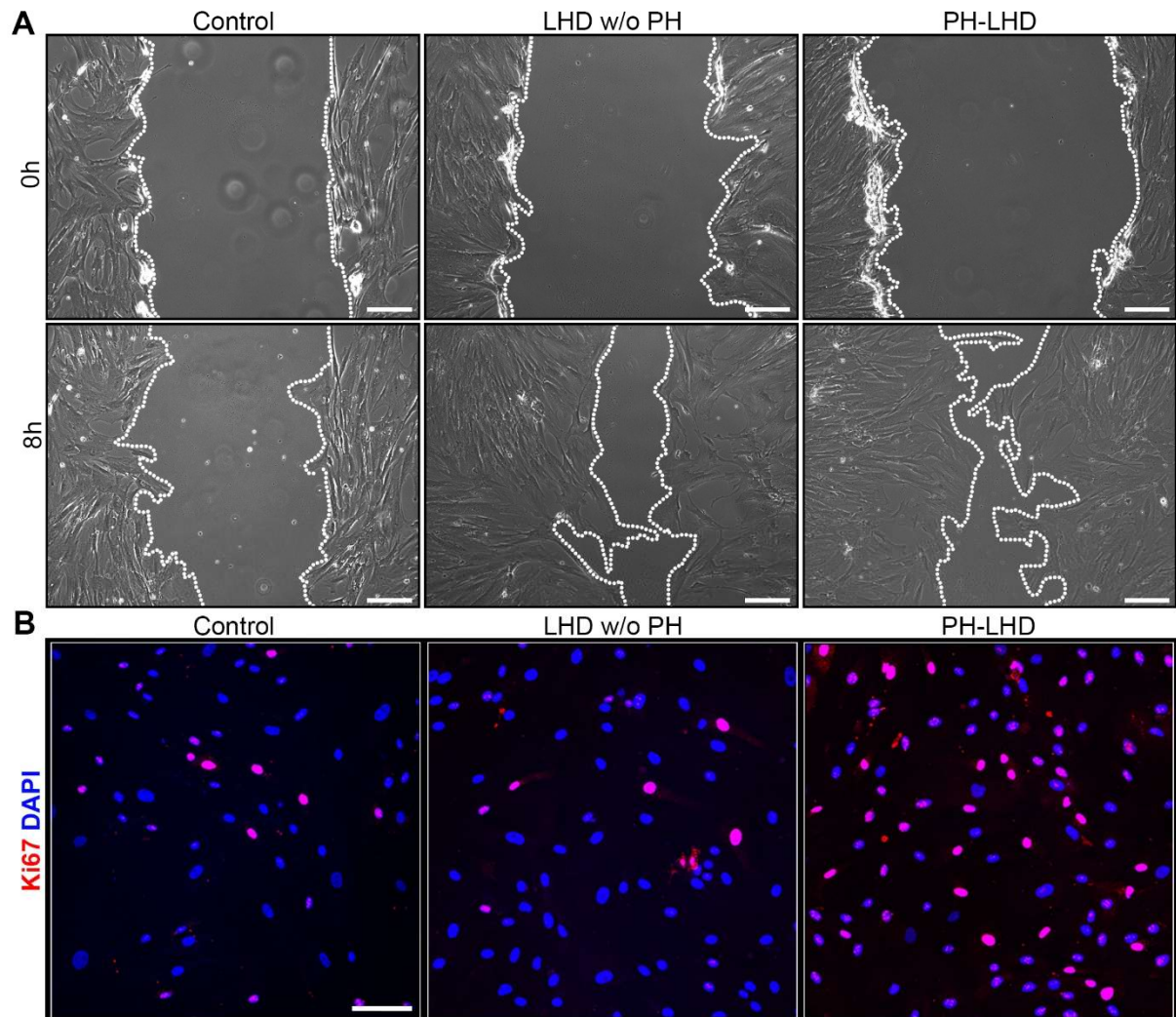
Antibody name, clone number	Host species	Company	Article number	Application (dilution)
Monoclonal anti- α smooth muscle actin, clone [1A4]	mouse	Abcam	ab7817	Immunofluorescence (1:200)
Monoclonal anti-collagen IV, clone [EPR7785]	rabbit	Abcam	ab6586	Immunofluorescence (1:200)
Polyclonal anti-laminin	rabbit	Thermo Fischer	PA1-16730	Western blotting (1:1000)
Polyclonal anti-laminin	rabbit	Abcam	ab11575	Immunofluorescence (1:200)
Monoclonal anti- β actin, clone [mAbcam 8226]	mouse	Abcam	ab8226	Western blotting (1:1000)
Polyclonal anti-Ki67	rabbit	Abcam	ab15580	Immunofluorescence (1:200)
Polyclonal anti-YAP1	rabbit	Thermo Fischer	PA5-86396	Immunofluorescence (1:200) Western blotting (1:1000)
Monoclonal anti-collagen I, clone [EPR7785]	rabbit	Abcam	ab138492	Western blotting (1:1000)
Monoclonal anti-human CD31 Alexa Fluor 594, clone [WM59]	mouse	Biolegend	303126	Immunofluorescence (1:500)
Monoclonal anti-paxillin, immunogen (aa. 1-557)	mouse	BD Biosciences	610619	Immunofluorescence (1:200)
Monoclonal anti-vinculin, immunogen (aa. 691-705)	rabbit	Sigma Aldrich	V4139	Immunofluorescence (1:1000)

Suppl. Table 2**Secondary antibodies**

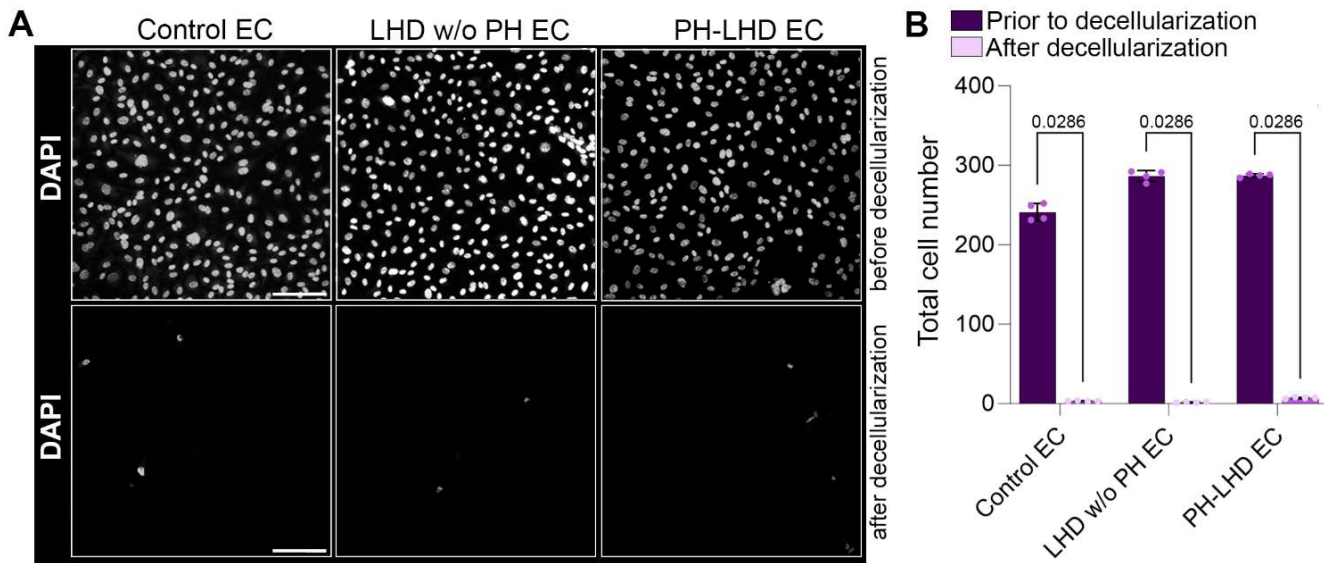
Antibody name	Host species	Company	Article number	Emission wavelength	Application (dilution)
Anti-mouse IgG (H+L) Alexa Fluor 488	goat	Thermo Fischer	A-11029	488	Immunofluorescence (1:500)
Anti-mouse IgG (H+L) Alexa Fluor 568	goat	Thermo Fischer	A-11004	568	Immunofluorescence (1:500)
Anti-mouse IgG (H+L) Alexa Fluor 647	goat	Abcam	ab150115	647	Immunofluorescence (1:500)
Anti-rabbit IgG (H+L) Alexa Fluor 488	goat	Abcam	ab150077	488	Immunofluorescence (1:500)
Anti-rabbit IgG (H+L) Alexa Fluor 568	goat	Thermo Fischer	A-11011	568	Immunofluorescence (1:500)
Anti-rabbit IgG (H+L) Alexa Fluor 647	goat	Thermo Fischer	A-21244	647	Immunofluorescence (1:500)
Anti-rabbit IgG (H+L) HRP	goat	Abcam	ab97080	-	Western blotting (1:10,000)
Anti-mouse IgG (H+L) HRP	goat	Abcam	ab6789	-	Western blotting (1:10,000)

Supplementary Figures

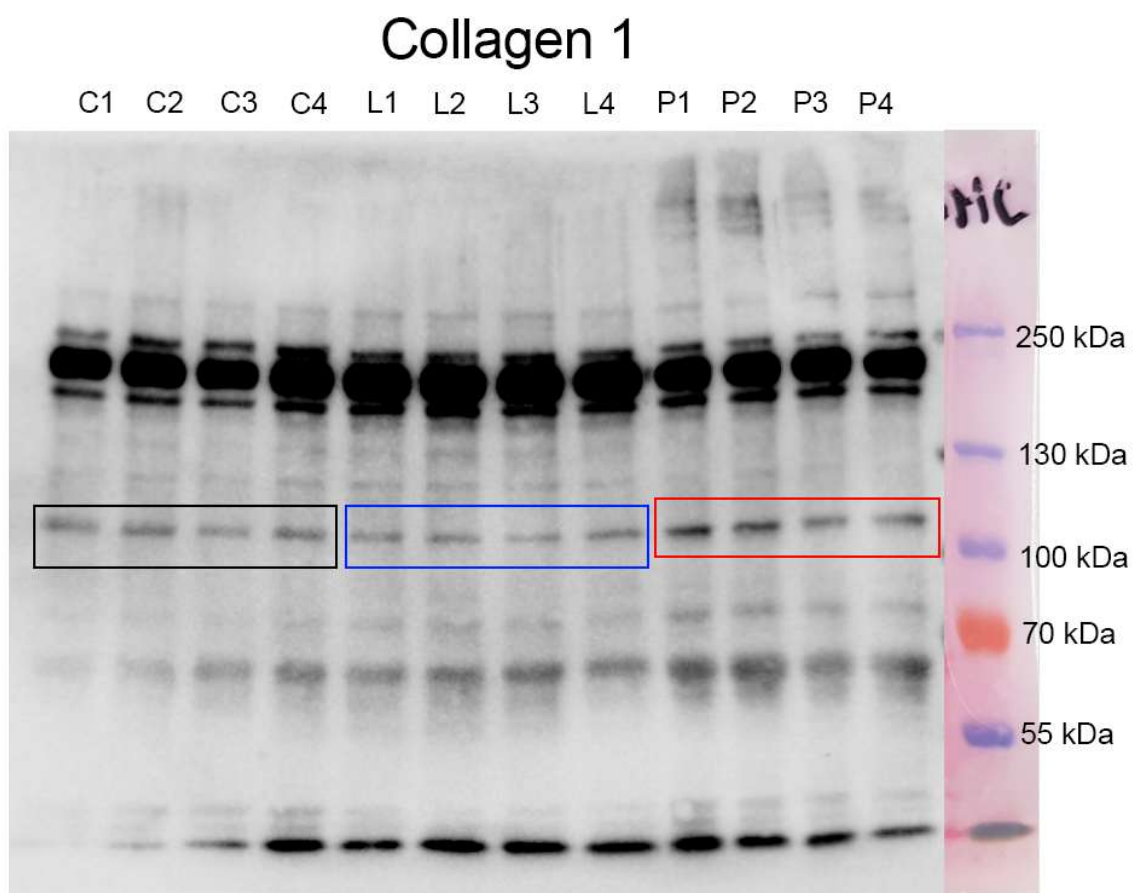
Supp. Figure 1



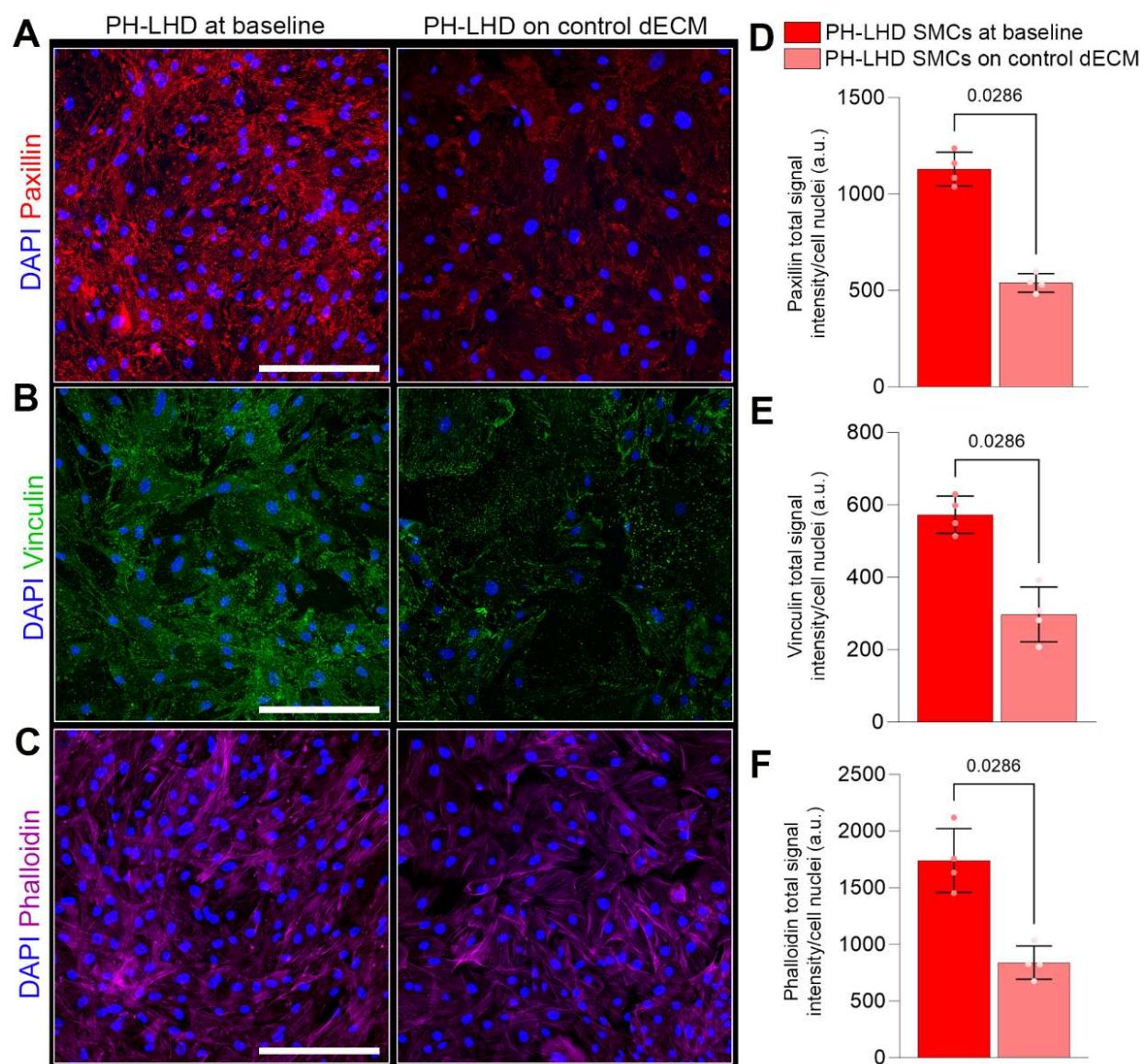
Supp. Figure 2



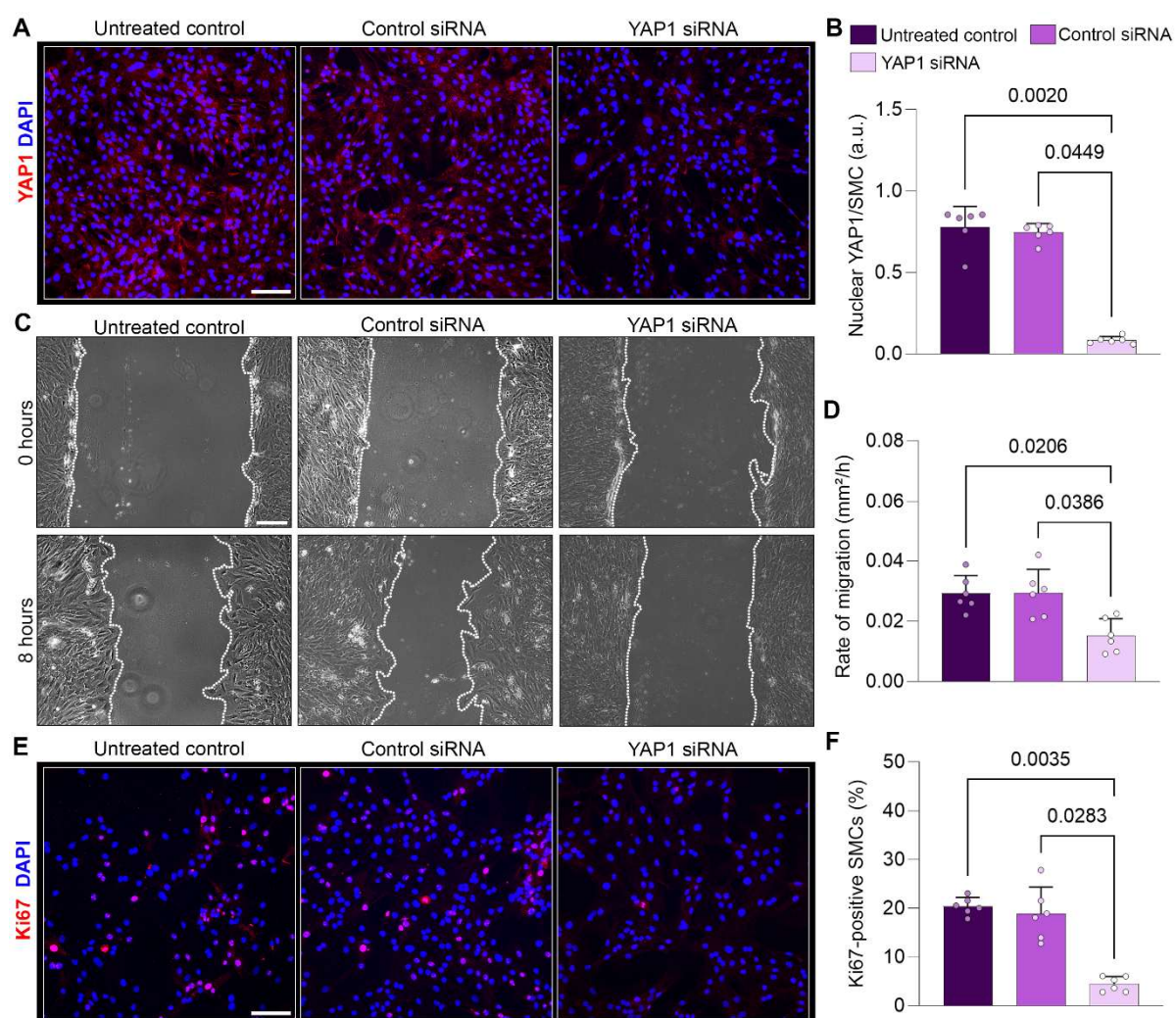
Suppl. Figure 3



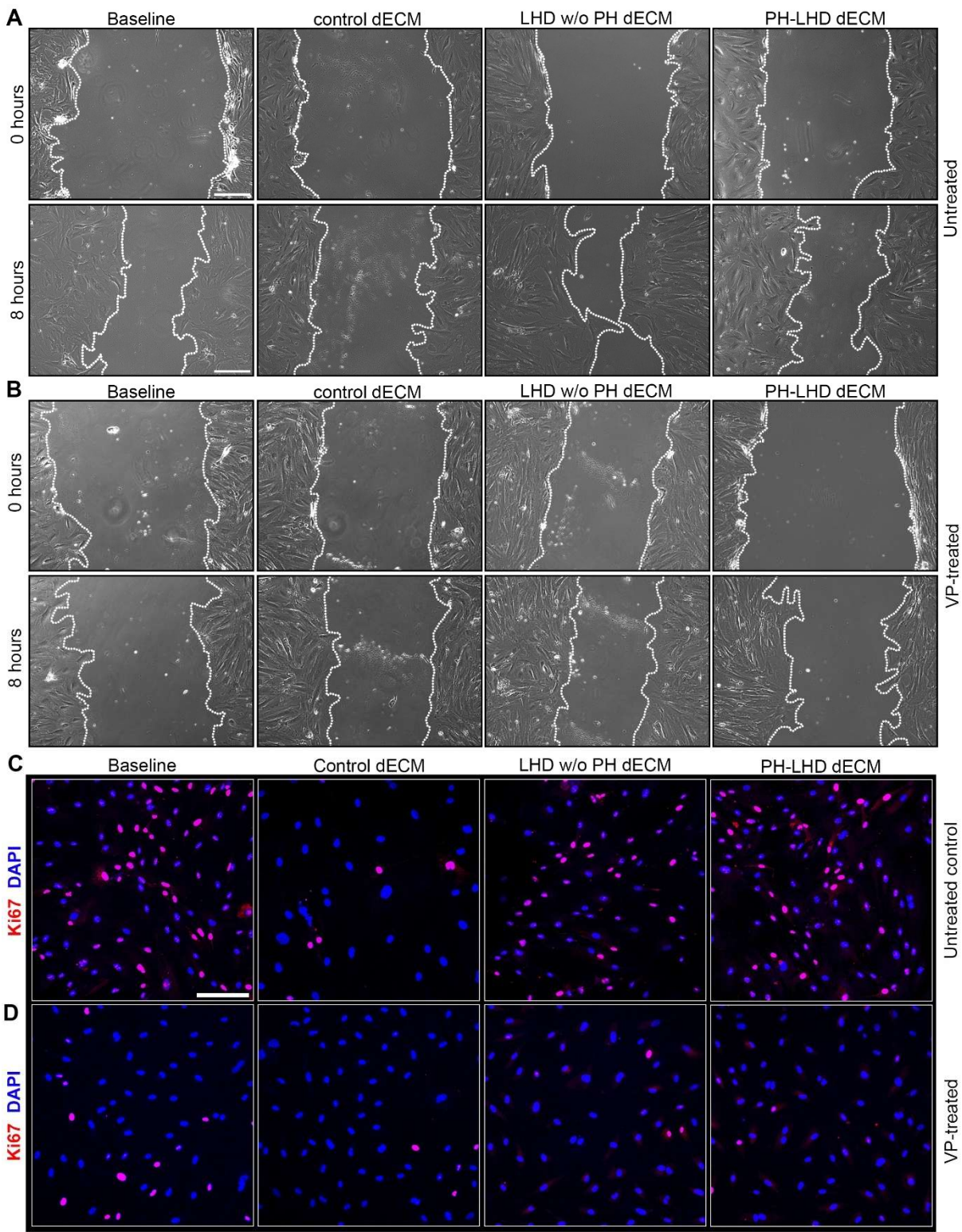
Suppl. Figure 4



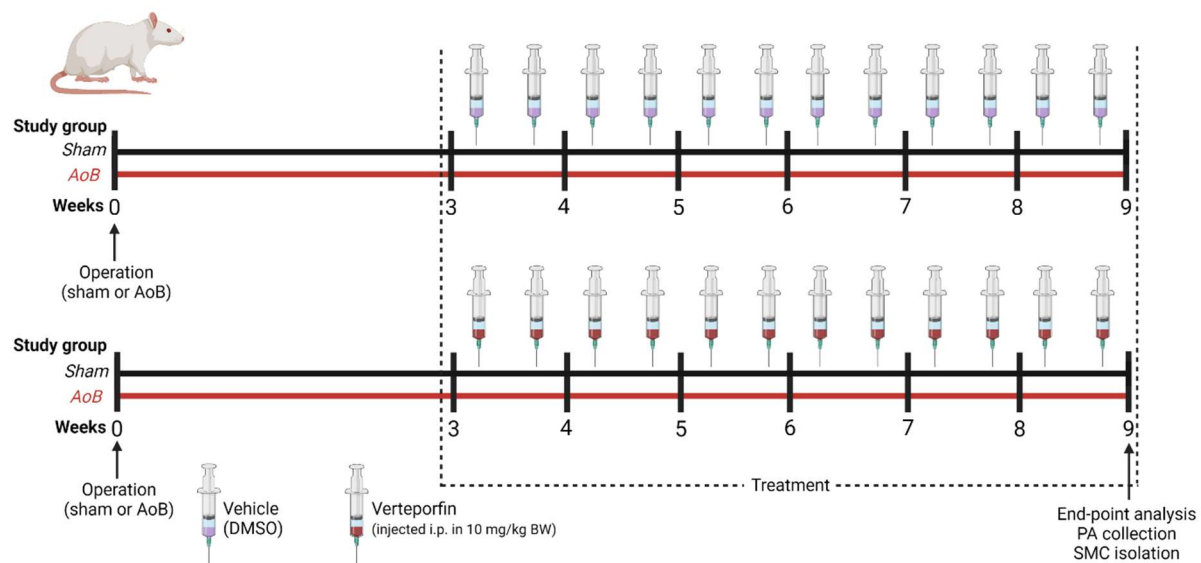
Suppl. Figure 5



Suppl. Figure 6



Suppl. Figure 7



References

1. Manz XD, Albers HJ, Symersky P, Aman J, van der Meer AD, Bogaard HJ, Szulcek R. In Vitro Microfluidic Disease Model to Study Whole Blood-Endothelial Interactions and Blood Clot Dynamics in Real-Time. *J Vis Exp* 2020.
2. Yan Y, He YY, Jiang X, Wang Y, Chen JW, Zhao JH, Ye J, Lian TY, Zhang X, Zhang RJ, Lu D, Guo SS, Xu XQ, Sun K, Li SQ, Zhang LF, Zhang X, Zhang SY, Jing ZC. DNA methyltransferase 3B deficiency unveils a new pathological mechanism of pulmonary hypertension. *Sci Adv* 2020; 6.
3. Hughes CS, Moggridge S, Muller T, Sorensen PH, Morin GB, Krijgsveld J. Single-pot, solid-phase-enhanced sample preparation for proteomics experiments. *Nat Protoc* 2019; 14: 68-85.
4. Rappsilber J, Ishihama Y, Mann M. Stop and go extraction tips for matrix-assisted laser desorption/ionization, nanoelectrospray, and LC/MS sample pretreatment in proteomics. *Anal Chem* 2003; 75: 663-670.
5. Pekayvaz K, Leunig A, Kaiser R, Joppich M, Brambs S, Janjic A, Popp O, Nixdorf D, Fumagalli V, Schmidt N, Polewka V, Anjum A, Knottenberg V, Eivers L, Wange LE, Gold C, Kirchner M, Muenchhoff M, Hellmuth JC, Scherer C, Rubio-Acero R, Eser T, Deak F, Puchinger K, Kuhl N, Linder A, Saar K, Tomas L, Schulz C, Wieser A, Enard W, Kroidl I, Geldmacher C, von Bergwelt-Baildon M, Keppler OT, Munschauer M, Iannacone M, Zimmer R, Mertins P, Hubner N, Hoelscher M, Massberg S, Stark K, Nicolai L. Protective immune trajectories in early viral containment of non-pneumonic SARS-CoV-2 infection. *Nat Commun* 2022; 13: 1018.
6. Justus CR, Leffler N, Ruiz-Echevarria M, Yang LV. In vitro cell migration and invasion assays. *J Vis Exp* 2014.
7. Grada A, Otero-Vinas M, Prieto-Castrillo F, Obagi Z, Falanga V. Research Techniques Made Simple: Analysis of Collective Cell Migration Using the Wound Healing Assay. *J Invest Dermatol* 2017; 137: e11-e16.
8. Kucherenko MM, Sang P, Yao J, Gransar T, Dhital S, Grune J, Simmons S, Michalick L, Wulsten D, Thiele M, Shomroni O, Hennig F, Yeter R, Solowjowa N, Salinas G, Duda GN, Falk V, Vyavahare NR, Kuebler WM, Knosalla C. Elastin stabilization prevents impaired biomechanics in human pulmonary arteries and pulmonary hypertension in rats with left heart disease. *Nat Commun* 2023; 14: 4416.
9. Liu SF, Kucherenko MM, Sang P, Li Q, Yao J, Nambiar Veetil N, Gransar T, Alesutan I, Voelkl J, Salinas G, Grune J, Simmons S, Knosalla C, Kuebler WM. RUNX2 is stabilised by TAZ and drives pulmonary artery calcification and lung vascular remodelling in pulmonary hypertension due to left heart disease. *Eur Respir J* 2024; 64.
10. Schindelin J, Arganda-Carreras I, Frise E, Kaynig V, Longair M, Pietzsch T, Preibisch S, Rueden C, Saalfeld S, Schmid B, Tinevez JY, White DJ, Hartenstein V, Eliceiri K, Tomancak P, Cardona A. Fiji: an open-source platform for biological-image analysis. *Nat Methods* 2012; 9: 676-682.